NANO LETTERS

2008
Vol. 8, No. 1
178−182

Mobile Iron Nanoparticle and Its Role in the Formation of SiO_2 Nanotrench via Carbon Nanotube-Guided Carbothermal Reduction

Hye Ryung Byon and Hee Cheul Choi*

Department of Chemistry, Pohang University of Science and Technology (POSTECH), San 31, Hyoja-Dong, Nam-Gu, Pohang, South Korea 790-784

Received September 17, 2007; Revised Manuscript Received December 3, 2007

ABSTRACT

The detailed role of iron nanoparticles (NPs) involved with the formation of SiO_2 nanotrenches is revealed. The physical movements of iron NPs, such as levitation and adsorption, turn out to be responsible for the initiation of carbothermal reduction (C (carbon nanotube, s) + SiO_2(s) ↔ SiO(g) + CO(g)), which results in SiO_2 nanotrenches that are fully guided by carbon nanotubes. Under the chemical vapor deposition condition with 0.1% of O_2 gas, iron NPs are liberally levitated from SiO_2/Si substrate then adsorbed on the sidewalls of carbon nanotubes. Depending on the numbers of iron NPs attached to carbon nanotubes, two different types of nanotrenches are determined. When multiple iron NPs are assembled on carbon nanotubes and involved in carbothermal reduction, aligned nanohole type of nanotrenches is produced (Type I). On the contrary, when single iron NPs initiate the carbothermal reduction, nanotrenches having smooth pathways and high shoulders are commonly formed (Type II).

Understanding chemical reactivity of carbon nanotubes is essential for their successful utilization in many potential applications. Most of the current researches dealing with chemical reactivity of carbon nanotubes are concentrated on their surface chemistry, such as noncovalent coatings of π-conjugated molecules through intermolecular $\pi-\pi$ interactions[1,2] and covalent couplings of functional molecules at the intentionally introduced defect sites on carbon nanotubes.[3] Recently, we have discovered a new intrinsic thermochemical reactivity of single-walled carbon nanotubes (SWNTs) by which solid SiO_2/Si surface is selectively etched via carbothermal reduction process.[4] The carbothermal reduction of SiO_2 is induced by sacrificing SWNTs when 0.1% of O_2 gas is added into the conventional iron catalyst nanoparticle (NP)-based chemical vapor deposition (CVD) condition where H_2, CH_4, and C_2H_4 gases are introduced at 900 °C for 10 min, by following C (carbon nanotube, s) + SiO_2(s) ↔ SiO(g) + CO(g). Although the trajectories of produced SiO_2 nanotrenches clearly mimic those of SWNTs in terms of shape, length, and width, they have rather wider width (∼10 nm) and deeper depth (∼5 nm) compared to the diameter of the original CVD-grown SWNT (∼1.7 nm) mainly because of further continuous reaction with externally provided hydrocarbon gases. The resulting SiO_2 nanotrenches hence are expected to be applied to, for example, Si-based nanoelectronic device fabrications.

The carbothermal reduction has never occurred under the conventional CVD condition, because the reaction between SWNTs and the SiO_2 surface normally requires high temperature (∼1700 °C)[5] due to its high activation energy. We have revealed that the activation energy could be significantly lowered by introducing defects in SWNTs during the reaction. To introduce defects, a small amount of O_2 gas has been supplied during the reaction,[6] and successful formation of nanotrenches has been observed at 900 °C.[4] Besides O_2 gas, we have also revealed that iron NPs catalyzing SWNT growth play a critical role as an initiator for the reaction by confirming that SiO_2 nanotrench has not been formed when Co catalyst NPs have been used under the identical reaction condition.[4,7] Although the "chemical" role of iron NP for nanotrench formation has been evidently revealed, its "physical" role has not been clearly understood yet. For example, it is still unclear if single or multiple iron NPs are responsible for the formation of nanotrenches. Herein, we report experimental evidence that supports the detailed roles of iron NPs in generation of SiO_2 nanotrenches.

Upon carbothermal reduction between SWNTs and underneath SiO_2 in O_2-assissted CVD condition, well-defined SiO_2 nanotrenches are mostly formed along the growing directions of SWNTs. At low-magnification atomic force

* Corresponding author. E-mail: choihc@postech.edu.

10.1021/nl072379u CCC: $40.75
Published on Web 12/21/2007

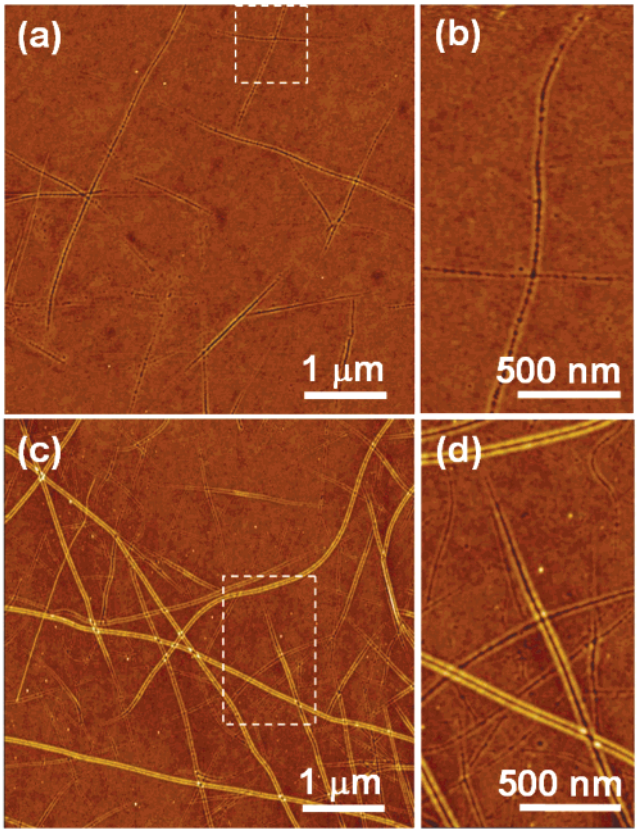

Figure 1. Representative AFM images of two distinctive types of nanotrenches. (a,b) Type I nanotrenches composed of nanohole arrays. (c,d) Type II nanotrenches having smooth and high shoulders without nanohole mark. Panels b and d are high magnification images of dashed boxes in panels a and c, respectively.

microscopy (AFM) images, most of the nanotrenches seem to have similar features as shown in Figure 1a,c. However, we have found that there are two distinctively different types of nanotrenches from high-magnification AFM images (Figure 1b,d). The first type of nanotrench consists of linearly aligned nanoholes (Type I, Figure 1b), while the other type has a smooth and straight pathway without any nanohole mark (Type II, Figure 1d). As also shown in the previous report,[4] Type II is mainly produced under the optimized carbothermal reduction condition (see Experimental Section 1 in Supporting Information), and it has two important features: (1) high shoulders and deep trenches and (2) no iron NPs found at either end points of the nanotrench. In contrast, Type I clearly shows that nanotrenches are formed by nanoholes aligned along the direction of SWNT growth (Figure 1b). Consequently, Type I nanotrenches have low and rough shoulders with shallow trenches. This unique Type I nanotrench would be possibly initiated and propagated only when multiple numbers of iron NPs are involved in the reaction.

Nanotrench Type I: Levitation of Iron NPs and Their Self-Assemblies on the Sidewalls of SWNTs. Occasionally, densely self-assembled iron NPs and aligned nanoholes along the SWNT trajectories are observed from the samples of carbothermal reductions, which are stopped after 5∼10 min. Figure 2a shows self-assembled iron NPs on the sidewalls of SWNTs after 5 min of reaction. We also have observed aligned nanoholes from another sample after 10 min of reaction as shown in Figure 2b−d.[8] To acquire more obvious evidence for these phenomena, we have investigated the movement of iron NPs and consequently formed nanoholes by monitoring the same positions before and after the reaction (Figure 2e,f) (see Experimental Section 2 in Supporting Information). In Figure 2e, self-assembled iron NPs on SWNTs are observed after 10 min of reaction. Most of iron NPs (or their clusters)[9] are adsorbed on the sidewalls of SWNTs at this stage. Upon further 10 min of reaction under the same condition, it is clearly shown that arrays of nanoholes are created (Figure 2f).

The above results imply that iron NPs are levitated, freely moving, and attracted to nearby SWNTs under O_2-assisted CVD process (Figure 2A). It should be noted that the levitating iron NPs are residual NPs sitting on SiO_2 surface, which have not been involved in the growth of carbon nanotubes. Furthermore, although many of the levitated NPs under the O_2-assisted CVD process are supposed to be vented out in the high gas flow rate (total 1521.5 sccm), significant numbers of levitated iron NPs are attracted and assembled on SWNTs. This unprecedented levitation phenomenon is quite surprising because no such levitation of iron NP has been observed during the conventional carbon nanotube growth reaction in which iron NPs behave as a simple reservoir for thermocatalytically pyrolized reactive hydrocarbon gases; therefore, iron NPs remain attached on the SiO_2 surface without moving. This indicates that the key factor enabling levitation of iron NP is O_2 gas. It has been reported that evaporation of iron takes place much easily by addition of low concentration of O_2 gas to inert gas at 1600 °C.[10−12] Furthermore, low partial O_2 pressure (less than 4 Torr) promotes volatilization of the SiO_2 with iron as a form of SiO(g) over at 1370 °C.[13,14] Nevertheless, the physical movement of iron NPs in carbothermal reduction environment has never been shown. In our case, when small amounts of O_2 gas are added, carbothermal reduction occurs on the iron NPs that are wrapped with amorphous carbons or graphitic layers.[15,16] The driving force for the levitation of iron NPs is believed to be such a feeble carbothermal reduction of the underneath SiO_2 by the carbon layers existing on iron NPs. As soon as the reduction starts, physical separation between iron NPs and SiO_2 occurs, which provides a chance for iron NPs to be levitated.

Nanotrench Type II: Formation of Nanotrenches from Single Iron NPs. While Type I nanotrenches have embossing-like shoulders and trenches because they are formed by aligned nanoholes generated from self-assembled iron NPs, Type II nanotrenches have high and smooth shoulders with deep trenches as representatively shown in Figure 1c,d. The formation of such a high shoulder is due to recondensed SiO gas, one of the gas products from carbothermal reduction, by the reaction with externally supplied O_2 gas ($SiO(g) + 1/2O_2(g) \leftrightarrow SiO_2(s)$).[4] Indeed, shallow and narrow SiO_2 nanotrenches with low shoulders are obtained when carbon feedstock gases are removed after the growth of SWNTs in CVD process, which eventually decreases the amounts of SiO gas (Figure S1 in Supporting Information). In addition,

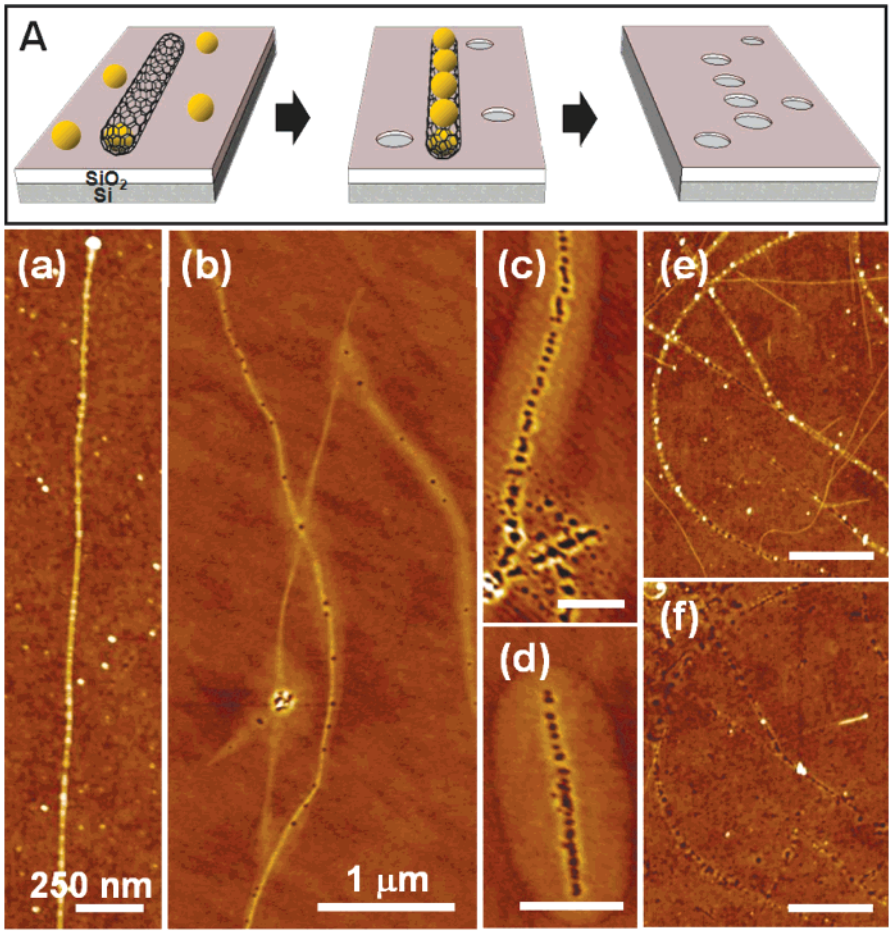

Figure 2. (A) Schematic view describing the mechanism responsible for the formation of Type I nanotrenches. (a) AFM image of self-assembled iron NPs on the sidewall of a SWNT. (b−d) Nanohole arrays along SWNT trajectories upon carbothermal reductions. (e,f) AFM images taken after 10 min of carbothermal reduction reaction (e) and after further 10 min of reaction (f) under O_2-assisted CVD condition with 1.5/300/1000/20/200 sccm of $O_2/H_2/CH_4/C_2H_4$/Ar gases. Scale bars in panels c−f are 500 nm.

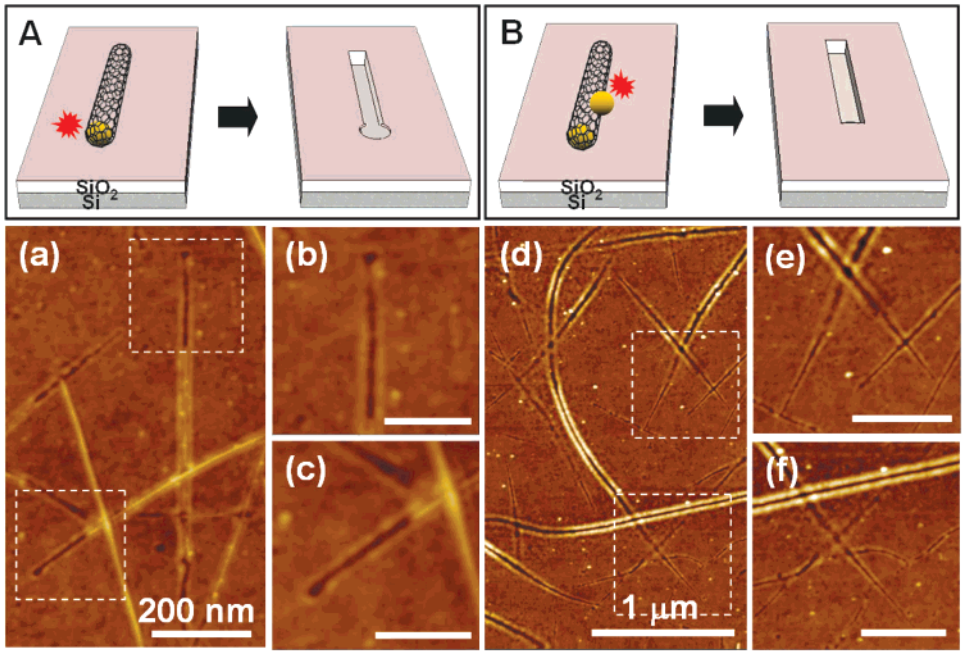

Figure 3. (A,B) Schematic views describing two mechanisms responsible for the formation of Type II nanotrenches. (a−c) AFM images of nanotrenches showing nanohole-connected trenches. Panels b and c are high magnification images of dashed boxes in panel a (scale bars are 100 nm). (d−f) AFM images of longer and deeper nanotrenches with high shoulders, but missing nanohole traces at either end of nanotrenches. Panels e and f are high magnification images of dashed boxes in panel d (scale bars are 400 nm).

this entails that single iron NPs are responsible for the formation of Type II nanotrenches.

Figure 3a−c shows single iron NP-driven Type II nanotrenches observed at the early stage of the reaction (after 5 min). Although nanotrenches are not fully developed at this stage, it is clearly confirmed that the initiation of carbothermal reduction process starts from the end of SWNTs where single iron NPs are originally located, resulting in single trace of nanoholes connected to nanotrenches. This result infers that iron NPs act as a catalyst for growth of SWNT, and the same iron NPs trigger carbothermal reduction as well (Figure 3A).

Meanwhile, when the reaction is allowed for straight 10 min, deeper and longer SiO_2 nanotrenches having high and smooth shoulders are formed in high population (Figure 3d−f). These nanotrenches are slightly different from the above-mentioned Type II nanotrenches because there is no evident trace of nanohole at one end of these nanotrenches (Figure 3e,f). It is quite acceptable to consider that the nanohole trace is not necessarily formed if formation of the nanotrench is initiated from the middle (instead of ends) of long SWNTs. Then, the question is how the carbothermal reduction can be initiated at the places where no iron NP is available. One plausible scenario is that one or several residual iron NPs are levitated and adsorbed on the sidewalls of the SWNTs like the Type I case (Figure 3B). In such a case, these few iron NPs tend to be removed immediately after initiating carbothermal reduction without nanohole trace because their chemical reactivity is much higher than the ones encapsulated in SWNTs,[17] and the reaction is self-propagated along the growth direction of SWNTs. Remember that when many iron NPs are densely adsorbed as in the case of Type I, iron NPs have more chance to generate nanoholes instead of nanotrenches due to strong longitudinal interactions among the NPs.

This postulate has been further confirmed by the following control experimental results (see Experimental Section 1 in Supporting Information). Figure 4 shows AFM images and schematic eye guidelines of trajectories projecting the same locations after 5 min (Figure 4a,b) and after successive additional 10 min of reaction (Figure 4g,h). While most of the original SWNTs generate SiO_2 nanotrenches, new nanotrenches are also created from newly grown SWNTs during the second 10 min of reaction. To investigate the initiating points of carbothermal reduction in detail, both ends of a certain nanotrench and the corresponding SWNT are monitored. The boxed areas of c and d in Figure 4a, and i and j in Figure 4g are magnified in Figure 4c,d,i,j, respectively. As clearly shown from the boxed areas in Figure 4i,j, both ends of a nanotrench are smoothly terminated without any iron NP trace after carbothermal reduction completes. As we have proposed, this nanotrench seems to be initiated by one of the several iron NPs adsorbed on the middle region of a SWNT (boxed areas in Figure 4c,d). Several iron NPs having ca. 1.30 (Figure 4e) and 1.72 nm (Figure 4f) of diameter are found attached on the SWNT after 5 min of reaction. These heights are comparable to diameters of iron NPs (1.2∼2.0 nm) deposited on SiO_2/Si substrates.

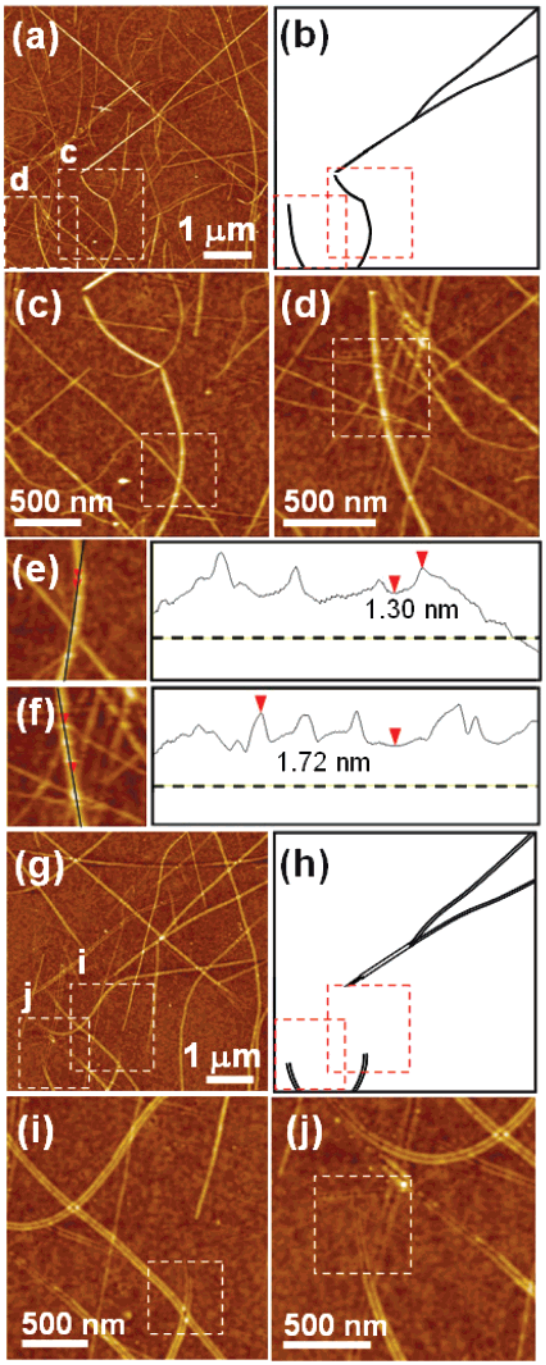

Figure 4. Time-dependent carbothermal reduction process monitored at same position of a sample. (a,b) AFM image of SWNTs after O_2-assisted CVD process for 5 min and its eye guideline, respectively. (c,d) High-magnification images of dashed boxes in panel a showing several iron NPs adsorbed on the SWNT. (e,f) Height profiles of dashed boxes in panels c and d, respectively. Height differences of two indicated red arrows are (e) 1.30 and (f) 1.72 nm. (g,h) AFM image of nanotrenches after 10 min of reaction more and its eye guideline, respectively. (i,j) High-magnification images of dashed boxes in panel g showing smooth ends of the nanotrench.

The Effect of the Number of Iron NPs for the Formation of SiO_2 Nanotrenches. As we have experimentally proven, iron NPs play a crucial role for the initiation and even propagation during the nanotrench formation. In particular, adsorption and self-assembly of levitated iron NPs

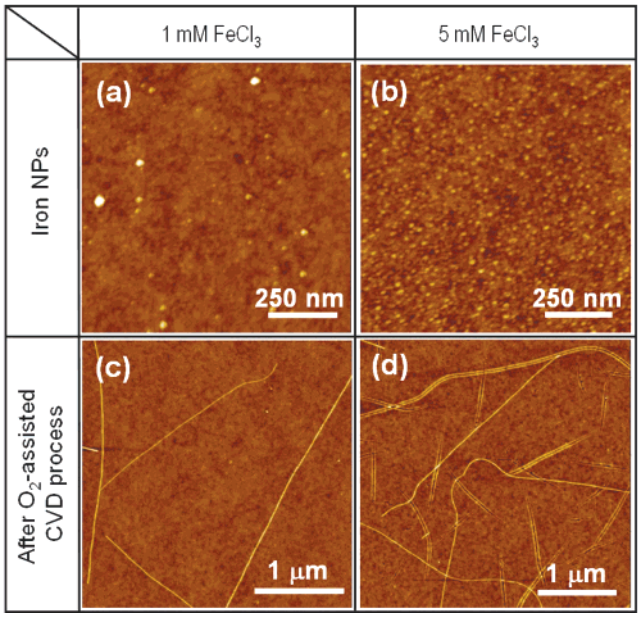

Figure 5. A correlation between the population of iron NPs and the formation of SiO_2 nanotrench. (a,b) AFM images of deposited iron NPs on SiO_2/Si substrates from 1 and 5 mM $FeCl_3$ solution, respectively. (c,d) AFM images after O_2-assisted CVD process for samples in panels a and b, respectively.

on the sidewalls of SWNTs turn out to be one of the most significant intermediating processes. The probability of such adsorption of iron NPs would be affected by the efficiency of their levitation from SiO_2 layer and ultimately by the population of iron NPs. To examine the correlation between the population of residual iron NPs and the formation of the nanotrench, we prepared two SiO_2/Si substrates on which iron NPs are deposited at different concentrations.

Figure 5 a,b shows iron NPs prepared by soaking SiO_2/Si substrates into 1 and 5 mM $FeCl_3$ solutions, and the numbers of iron NPs are roughly counted around 100 and 1200 per 1 μm^2, respectively. After 10 min of reaction, no nanotrench is formed from the sample containing low population of iron NPs and instead only SWNTs are grown. (Figure 5c). On the other hand, deep and clear nanotrenches are produced from the sample containing high population of iron NPs (Figure 5d). These results indicate that the opportunity for iron NPs to be levitated and adsorbed on SWNTs is dramatically decreased when the population of iron NP is low (less than 100 iron NPs per 1 μm^2). On the contrary, such a chance is increased as the population of available iron NPs is increased, guaranteeing high efficiency of carbothermal reduction.[18] No significant difference in terms of influence and efficiency of iron NPs is observed upon further increase of iron NP population.

In conclusion, we have shown that two different types of SiO_2 nanotrenches are created by two independent mechanisms during carbothermal reduction reaction between SWNTs and underneath SiO_2 substrate. The key factor involved in the determination of these two mechanisms is iron NPs. Nanotrenches composed of embossing-like nanohole arrays are formed by numerous NPs that are self-assembled on the sidewalls of SWNTs (Type I). The unprecedented self-assembly of multiple iron NPs occurs as residual iron NPs are levitated from the SiO_2 surface and attracted to nearby SWNTs under the O_2 gas-presented CVD environment. In contrast, the formation of smooth and straight nanotrenches is initiated by single iron NPs (Type II).

Acknowledgment. This work was supported by Nano/Bio Science & Technology Program of MOST (2006-00955), KOSEF 2007-8-1158, and Korean Research Foundation (MOEHRD, KRF-2005-005-J13103).

Supporting Information Available: Experimental details and Figure S1. This material is available free of charge via the Internet at http://pubs.acs.org.

References

(1) Chen, R. J.; Zhang, Y.; Wang, D.; Dai, H. *J. Am. Chem. Soc.* **2001**, *123*, 3838.
(2) Tournus, F.; Latil, S.; Heggie, M. I.; Charlier, J.-C. *Phys. Rev. B* **2005**, *72*, 075431.
(3) Tasis, D.; Tagmatarchis, N.; Bianco, A.; Prato, M. *Chem. Rev.* **2006**, *106*, 1105.
(4) Byon, H. R.; Choi, H. C. *Nat. Nanotechnol.* **2007**, *2*, 162.
(5) Koc, R.; Cattamanchi, S. V. *J. Mater. Sci.* **1998**, *33*, 2537.
(6) Li, J.-L.; Kudin, K. N.; McAllister, M. J.; Prud'homme, R. K.; Aksay, I. A.; Car, R. *Phys. Rev. Lett.* **2006**, *96*, 176101.
(7) Byon, H. R.; Lim, H.; Song, H. J.; Choi, H. C. *Bull. Korean Chem. Soc.* **2007**, *28*, 2056.
(8) Reproducibility of syntheses for self-assembled iron NPs and aligned nanoholes is less than 5% under optimized condition. Therefore, a new specific reaction condition has been developed for reproducible self-assembly of iron NPs (see Experimental Section 2 in Supporting Information).
(9) Most of the self-assembled iron NPs have much larger diameters (2∼10 nm) than the residual iron NPs (1∼2 nm) originally deposited on SiO_2/Si substrate.
(10) Turkdogan, E. T.; Grieveson, P.; Darken, L. S. *J. Phys. Chem.* **1963**, *67*, 1647.
(11) Yokoyama, S.; Saito, K.; Ito, N.; Kawakami, M. *J. Jpn. Inst. Met.* **1995**, *59*, 814.
(12) Yokoyama, S.; Saito, K.; Ito, N.; Kawakami, M. *J. Jpn Inst. Met.* **1995**, *59*, 1030.
(13) Boyer, S. M.; Moulson, A. J. *J. Mater. Sci.* **1978**, *13*, 1637.
(14) Moulson, A. J. *J. Mater. Sci*. **1979**, *14*, 1017.
(15) Li, Y.; Kim, W.; Zhang, Y.; Rolandi, M.; Wang, D.; Dai, H. *J. Phys. Chem. B* **2001**, *105*, 11424.
(16) Hofmann, S.; Sharma, R.; Ducati, C.; Du, G.; Mattevi, C.; Cepek, C.; Cantoro, M.; Pisana, S.; Parvez, A.; Cervantes-Sodi, F.; Ferrari, A. C.; Dunin-Borkowski, R.; Lizzit, S.; Petaccia, L.; Goldoni, A.; Robertson, J. *Nano Lett.* **2007**, *7*, 602.
(17) Chen, W.; Pan, X.; Bao, X. *J. Am. Chem. Soc.* **2007**, *129*, 7421.
(18) Shimoo, T.; Kobayashi, Y. *J. Jpn. Inst. Met.* **1992**, *56*, 45.

NL072379U